of brine heterogeneity in modern sedimentary basins (6) imply inefficiency of mixing and the potential for preservation of individual, metal-charged brine reservoirs that could be tapped at some later time.

In the case of Ireland, the origin of metal-enriched fluids is uncertain, although a deepening convective flow system (15) has the capability to extract higher concentrations of metal later in the life of the system due to increasing temperature and possibly also progressive exhaustion of the buffer capacity for pH (by feldspar-mica) or the activity of H_2S (by pyrite-Fe silicate) on the convective flow path. The observation that the texturally later brines have higher metal contents is consistent with this model, although their higher salinity is also likely to have contributed to enhanced metal transport. The high Ba content of the metalliferous fluids (up to 6000 ppm) indicates that the oxidized sulfur content must have been low, limited by barite saturation. Combined with high base metal concentrations that imply low reduced sulfur concentrations, we conclude that a key property of these fluids was low ΣS (total sulfur concentration).

High metal concentrations may pertain in other types of hydrothermal ore systems, such as epithermal or volcanic-hosted massive sulfide deposits. In these environments, periodic injection of metalliferous magmatic fluids may be responsible for the bulk of metal introduction (28–30) into systems otherwise dominated by barren geothermal waters. A number of large, high-temperature, magmatic-hydrothermal deposits are also known to have formed from magmatic fluids that contained very high concentrations of ore metals (31–33). Accepting that hydrothermal ores may form specifically from anomalously metal-rich batches of fluid implies geochemically specialized source regions and an episodicity and potentially short duration of ore-forming events that may be controlled by changes in hydrology. Although the existence of an efficient trap for these metals remains a fundamental prerequisite for hydrothermal ore formation, our interpretation contrasts with the view that many crustal fluids are viable ore fluids subject to the right perturbations in physicochemical conditions to cause efficient deposition (24).

References and Notes

1. H. L. Barnes, A. W. Rose, Science **279**, 2064 (1998).
2. D. L. Huston, J. Aust. Geol. Geophys **17**, 15 (1998).
3. T. M. Seward, H. L. Barnes, in Geochemistry of Hydrothermal Ore Deposits, H. L. Barnes, Ed. (Wiley, New York, ed. 3, 1997), pp. 435–486.
4. J. S. Hanor, in Carbonate-Hosted Lead-Zinc Deposits, Society of Economic Geologists Spec. Publ. 4 (Society of Economic Geologists, Littleton, CO, 1996), pp. 483–500.
5. K. L. Von Damm, Annu. Rev. Earth Planet. Sci. **18**, 173 (1990).
6. M. A. McKibben, L. A. Hardie, in Geochemistry of Hydrothermal Ore Deposits, H. L. Barnes, Ed. (Wiley, New York, ed. 3, 1997), pp. 877–936.
7. G. Garven, M. S. Appold, V. I. Toptygina, T. J. Hazlett, Hydrogeol. J. **7**, 108 (1999).
8. M. S. Appold, G. Garven, Econ. Geol. **95**, 1605 (2000).
9. C. J. Hodgson, in Giant Ore Deposits, Society of Economic Geologists Spec. Publ. 2 (Society of Economic Geologists, Queens Univ., Golden, CO, 1993), pp. 1–2.
10. E. Roedder, Fluid Inclusions, Reviews in Mineralogy, vol. 12 (Mineralogical Society of America, Washington, DC, 1984).
11. J. J. Wilkinson, Lithos **55**, 229 (2001).
12. A. R. Campbell, K. S. Panter, Geochim. Cosmochim. Acta **54**, 673 (1990).
13. J. G. Viets, A. H. Hofstra, P. Emsbo, in Carbonate-Hosted Lead-Zinc Deposits, Society of Economic Geologists Spec. Publ. 4 (Society of Economic Geologists, Littleton, CO, 1996), pp. 465–482.
14. D. L. Leach, in Sediment-Hosted Zn-Pb Ores (Springer, Berlin, 1994), pp. 104–138.
15. M. J. Russell, in Geology and Genesis of Mineral Deposits in Ireland (Irish Association for Economic Geology, Dublin, 1986), pp. 545–554.
16. J. J. Wilkinson, C. E. Everett, A. J. Boyce, S. A. Gleeson, D. M. Rye, Geology **33**, 805 (2005).
17. B. Stoffell, M. S. Appold, J. J. Wilkinson, N. A. McClean, T. E. Jeffries, Econ. Geol. **103**, 1411 (2008).
18. C. E. Everett, J. J. Wilkinson, D. M. Rye, in Fractures, Fluid Flow and Mineralization, Geological Society of London Spec. Publ. 155 (Geological Society of London, London, 1999), pp. 247–276.
19. I. M. Samson, M. J. Russell, Econ. Geol. **82**, 371 (1987).
20. Materials and methods are available as supporting material on Science Online.
21. B. Stoffell, J. J. Wilkinson, T. E. Jeffries, Am. J. Sci. **304**, 533 (2004).
22. T. E. Jeffries, S. E. Jackson, H. P. Longerich, J. Anal. At. Spectrom. **13**, 935 (1998).
23. M. S. Appold, T. J. Numelin, T. J. Shepherd, S. R. Chenery, Econ. Geol. **99**, 185 (2004).
24. B. Yardley, Econ. Geol. **100**, 613 (2005).
25. A. B. Carpenter, M. L. Trout, E. E. Pickett, Econ. Geol. **69**, 1191 (1974).
26. Y. K. Kharaka et al., Appl. Geochem. **2**, 543 (1987).
27. K. C. Benison, R. H. Goldstein, B. Wopenka, R. C. Burruss, J. D. Pasteris, Nature **392**, 911 (1998).
28. S. F. Simmons, K. L. Brown, Science **314**, 288 (2006).
29. C. A. Heinrich, Science **314**, 263 (2006).
30. T. Ulrich, S. D. Golding, B. S. Kamber, K. Zaw, Ore Geol. Rev. **22**, 61 (2003).
31. T. Ulrich, D. Günther, C. A. Heinrich, Nature **399**, 676 (1999).
32. A. C. Harris, V. S. Kamenetsky, N. C. White, E. van Achterbergh, C. G. Ryan, Science **302**, 2109 (2003).
33. B. Rusk, M. Reed, J. H. Dilles, L. Klemm, C. A. Heinrich, Chem. Geol. **210**, 173 (2004).
34. This work was supported by an Imperial College Albert Julius Bursary to B.S. and National Environment Research Council grant GR9/03047. We thank B. Coles and R. Garcia-Sanchez for laboratory support and the Natural History Museum–Imperial College London Joint Analytical Facility for access to instrumentation. The constructive comments of three anonymous reviewers are appreciated.

Signature of the End-Cretaceous Mass Extinction in the Modern Biota

Andrew Z. Krug,[1] David Jablonski,[1] James W. Valentine[2]

The long-term effects of mass extinctions on spatial and evolutionary dynamics have been poorly studied. Here we show that the evolutionary consequences of the end-Cretaceous [Cretaceous/Paleogene (K/Pg)] mass extinction persist in present-day biogeography. The geologic ages of genera of living marine bivalves show a significant break from a smooth exponential distribution, corresponding to the K/Pg boundary. The break reflects a permanent increase in origination rates, intermediate between the Mesozoic rate and the post-extinction recovery pulse. This global rate shift is most clearly seen today in tropical bioprovinces and weakens toward the poles. Coupled with the modern geographic distributions of taxa originating before and after the K/Pg boundary, this spatial pattern indicates that tropical origination rates after the K/Pg event have left a permanent mark on the taxonomic and biogeographic structure of the modern biota, despite the complex Cenozoic history of marine environments.

The major extinctions of the geologic past, each of which removed >50% of well-preserved genera and perhaps >70% of their species (1, 2), irreversibly restructured the taxonomic composition of the global biota. Although the broad macroevolutionary consequences of mass extinctions are well known (as in the dinosaurs-mammals changeover), their long-term effects on the temporal and spatial dynamics of clades and biotas are rarely investigated. For example, the good fit of modern biodiversity to local temperatures and to refugia from recent glaciations (3, 4) might imply that the recovery from the most recent major extinction, at the end of the Cretaceous Period 65 million years ago (Ma) [the Cretaceous/Paleogene (K/Pg) extinction], is largely obscured by subsequent events.

Here, we show the lasting influence of the K/Pg mass extinction on the evolutionary and biogeographic structure of modern biotas, using backward survivorship curves (BSCs, also called prenascence curves), which plot the proportion of taxa within a cohort that originated before some reference time (5, 6). Assuming that rates are time-specific and taxonomically homogeneous (5), a BSC defines an exponential probability function governed only by the origination rate (λ) of the cohort (7). The slope of a BSC is insen-

[1]Department of Geophysical Sciences, University of Chicago, 5734 South Ellis Avenue Chicago, IL 60637, USA. [2]Department of Integrative Biology and Museum of Paleontology, University of California, Berkeley, Berkeley, CA 94720, USA.

sitive to variations in extinction rate, so any significant changes in that slope signal major shifts in the origination rate (5). BSCs are particularly useful here because they let us (i) estimate intrinsic rates within bivalve cohorts, as opposed to a building a time series of individual events; and (ii) analyze the structure of age-frequency distributions in modern biotic provinces in comparison to the global distributions.

We analyzed (7) a taxonomically standardized, spatially explicit, global database of shallow-water living marine bivalves (8, 9), which now includes 73 families (table S1), 854 genera and subgenera (711 with a fossil record), 5132 species, and 28,264 spatial occurrences from 322 localities (fig. S1). Marine bivalves are one of the few groups that allow a direct analysis of long-term evolutionary and biogeographic dynamics: They have a rich and spatially extensive fossil record, their systematics are increasingly well known and standardized, and imperfections in their record are increasingly understood in terms of preservational controls (10–15). Their diversity patterns today and through the Cenozoic correspond closely to those of other major marine clades, both spatially and temporally (16, 17), and so they are a robust model system for probing the evolutionary and biogeographic history of the global biota. Localities were grouped into provinces according to sources cited in (7). BSCs were constructed (5, 18, 19) using the geologic ages of genera in an extensively revised and updated version of Sepkoski's compendium (8, 10, 20). We tested the fit of one-parameter, three-parameter, and five-parameter probability functions (7) to the global and provincial data, using the *optim* function in the software package R.

The BSC for extant bivalves globally shows a distinct inflection point at ~65 Ma (Fig. 1, A and B), with an increase in origination rate (λ) after the mass extinction (from 0.015 to 0.029 genera per lineage per million years) that continues to the present. A three-parameter model, incorporating two probability functions (with rate parameters λ_1 and λ_2; see methods in supporting online material) describing the BSC on either side of the inflection point (t_{crit}), is statistically supported over a single exponential fit (table S1). The optimizations place the inflection point near the K/Pg boundary, maximally supporting an age of 69 million years (My), not distinct from the K/Pg boundary, given the resolution of our binning scheme (7); the difference between the support of a critical age of 65 versus 69 My is not statistically meaningful (fig S2). This slight offset may also reflect less intense study in the 75- to 100-My interval, which could artificially concentrate originations in the last 10 My of the Cretaceous (2). This result indicates a significant and permanent increase in the origination rate of extant marine bivalve clades after the K/Pg extinction.
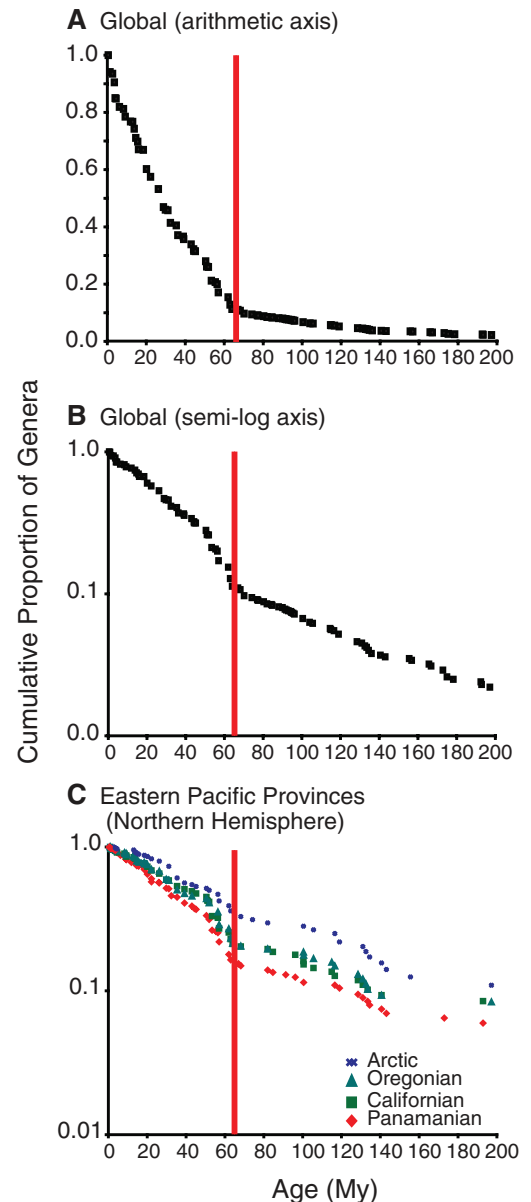
A discrete rebound phase with a steeper slope is also visible in semi-log space for the global data set (Fig. 1B), verified by a five-parameter (three rate parameters and two inflection points)

model with a slope of 0.065 (four times the Mesozoic value and twice the overall Cenozoic value) and bounded at 65 and ~50 Ma. This short-term origination pulse is consistent with patterns described for post-K/Pg bivalves (21) and for other post-extinction intervals, and patterns of diversification in recovery episodes clearly stand as distinct from those in more quiescent times. However, this transient increase in origination does not bias the estimated rate differential between the broader Mesozoic and Cenozoic intervals. The rate estimated for the final 50 My of the Cenozoic (0.026) is very similar to that for the entire Cenozoic (0.030), indicating that the overall Cenozoic rate, λ_1 estimated with the three-parameter model above (table S2), is mathematically dominated by the shift in "normal" origination rates rather than the post-extinction rebound interval.

The evolutionary signature of the K/Pg event is also seen at the provincial scale (Figs. 1C and

2), with a strong latitudinal component despite the apparent global homogeneity of the extinction itself (22). The three-parameter function, with an inflection point near the K/Pg boundary, is the optimal fit for 19 of the 27 provinces; the provincial curves show some additional variation, but minor inflection points are not supported when the five-parameter model is used (perhaps due to small sample sizes in provinces with additional non-K/Pg inflections, such as the Lusitanian; Fig. 2). Provincial values of λ decrease with latitude (Fig. 1C), so that a one-parameter exponential function is best supported for two polar and six high-latitude provinces (table S2). This latitudinal effect is seen most clearly when a critical time of 65 My is imposed on all 27 provinces and the probability functions are fit to the data: The difference between the post- and pre-K/Pg rates ($\lambda_1 - \lambda_2$) declines significantly as the latitudinal midpoint of the province increases (Fig. 3A), a pattern driven predominantly by the

Fig. 1. Global and regional BSCs for living marine bivalves; the vertical red line marks the K/Pg boundary (65 Ma). (**A**) Global BSC plotted on arithmetic axes. (**B**) Global BSC in semi-log space showing constant rates and different slopes of the pre- and post-K/Pg portions of the curve. Straight lines in semi-log space represent constant exponential rates. (**C**) Decrease in BSC slopes with increasing latitude for the Northern Hemisphere bioprovinces of the eastern Pacific.

A Global (arithmetic axis)

B Global (semi-log axis)

C Eastern Pacific Provinces (Northern Hemisphere)

Arctic
Oregonian
Californian
Panamanian

Age (My)

Cumulative Proportion of Genera

shallowing of the estimated Cenozoic rate (λ_1) in high-latitude provinces (Fig. 3B). Pre-K/Pg rates show no such latitudinal trend (Fig. 3C). The tropical West Pacific and Arctic provinces show the extremes of this contrast (fig. S3): The pre-K/Pg slopes of these two provinces differ only slightly (many of these older taxa are shared by the two regions), but the difference after the K/Pg extinction is dramatic.

The ages used here are the global first appearance of a genus (as opposed to the first occurrence of a genus in a given province), so that the slope of the provincial curves represents the outcome of origination plus invasion minus local extinction, rather than simple in situ origination. However, the late Cenozoic fossil record con-

strains these data by showing that marine bivalve genera tend to appear first in the tropics, with range expansion being overwhelmingly unidirectional from the tropics to the poles (8, 9, 23). The shallowing of Cenozoic age-frequency curves from tropics to poles thus appears to reflect the decreasing probability for genera to reach and remain established in progressively higher latitudes (9). Therefore, though the end-Cretaceous extinction was equally severe in low and high latitudes (22), the spatial pattern of origination and spread affects the taxonomic structures of these regions differently; the post-K/Pg slopes of BSCs primarily reflect origination rates in tropical provinces and invasion rates in polar provinces. This view is supported by the contrasting

geographic distributions of pre- and post-K/Pg genera (Fig. 4). The distribution of post-K/Pg genera today forms a hollow curve, with 32% of the 638 genera being present exclusively in tropical or warm-temperate provinces (Fig. 4). Pre-K/Pg genera have significantly wider distributions, with only 14% of 73 genera being exclusive to warm-water provinces (significantly fewer than in the post-K/Pg sample, log-likelihood ratio G test, $P < 0.001$), the majority (82%) inhabiting both warm- and cold-water regions (Fig. 4).

Because the present day is our reference time, our BSCs are reminiscent of lineage-through-time (LTT) plots, which estimate diversity dynamics through time using the divergence times of lineages in a phylogenetic tree constructed for

Fig. 2. Backward survivorship curves for the 27 provincial faunas of the present-day shelf biota. Plots are on arithmetic axes to enable visualization at low diversities; vertical red lines mark the K/Pg boundary (65 Ma).
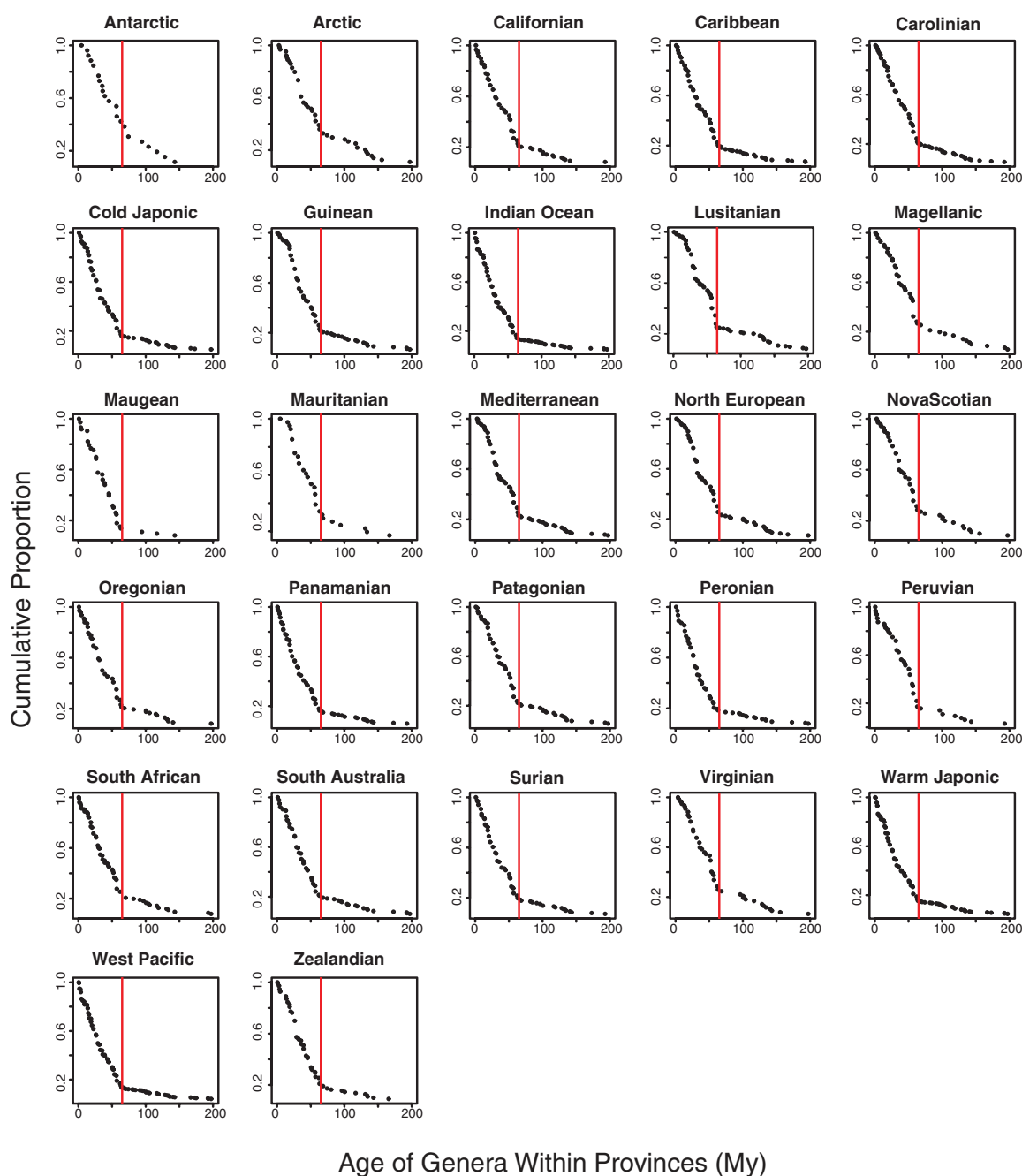
living species (24–27). BSCs differ importantly from LTTs, however, in that the frequency distribution of branch lengths (here the age of the genus) is the raw data, rather than the length of time between nodes on a phylogenetic tree (28). Therefore, although changes in extinction rate can influence the slopes of LTTs (24, 28), these effects are mathematically cancelled out in BSCs (5, 28), given the assumptions noted above.

Nevertheless, we verified our global results by calculating the average per-taxon origination rates (29) [termed "per-capita rates" in (29), but units are actually per lineage per million years] of all genera, living and extinct, within extant bivalve families for 5-My intervals within the post-recovery Cenozoic (0 to 50 Ma) and for the 50 My before the K-Pg boundary. This form of per-capita rate, derived from branching theory, is robust to variation in the true extinction rate, including events as dramatic as mass extinctions (29). Focusing on shorter 5-My intervals also limits the biasing effect of taxonomic heterogeneity on the estimated rates, so this analysis, including extinct genera, makes a useful comparison to the results for living genera alone. These per-capita origination rates are remarkably close to those determined for the living genera, with the rate for the 50 My before the K/Pg at 0.020 genera per lineage per million years (versus 0.014 for the living cohort) and the

post-K/Pg rate at 0.026 per lineage per million years (versus 0.026 for the living cohort), a statistically significant increase (Student's t test, P = 0.02, normality of data confirmed by Shapiro-Wilk test; a nonparametric Wilcoxon signed-rank test gives a similar result, P = 0.025) that corroborates the shift in origination rate at the K/Pg boundary. The per-taxon rate calculations do not specifically address the assumptions underlying the rates estimated from the BSC of the living cohort, but the agreement of the two results suggests that the inference of an inflection point in the BSC is robust. Spatially explicit LTT plots and paleontological cohort analyses will be valuable next steps but are difficult to generate because local extinction rates can include strong sampling effects.

The sharp increase in the slope of the bivalve BSC after the K/Pg event is unlikely to derive entirely from improved preservation and sampling in the younger part of the record and in the present day. Our optimizations find the changes in slope at the K/Pg boundary and in the early Eocene, not in the late Cenozoic when lithification and dissolution impinge least on fossil preservation (30). Additionally, an analysis restricted to bivalves having shell microstructures most robust to geochemical dissolution (with low organic content, consisting predominantly of calcite) and thus producing records least subject to dis-

tortion over time (11) shows a pattern consistent with that of the entire bivalve cohort (fig. S4).

These results provide a long-term perspective on the consequences of the K/Pg mass extinction, with a significant shift in origination rate that outlasted the accelerated recovery phase, and a strong spatial component to diversification, such that tropical and warm-temperate regions carry the strongest signature of post-K/Pg evolution. The lasting increase in origination may reflect the removal of competitors or predators that were damping the Mesozoic diversification of the living families; alternatively, the Cenozoic diversification of shell-penetrating predators, particularly in the tropics (31, 32), might have increased origination rates in their prey during the post-recovery interval. These hypotheses need to be tested directly; for example, by ecological and functional analyses of victims and post-extinction diversifiers. The declining strength of the apparent shift in global origination rates with latitude underscores how the taxonomic composition of high-latitude provinces depends on tropical origination rates. The K/Pg extinction was large, but its downstream effect has also been important

Fig. 3. Relationship between the estimated rates for the 27 biogeographic provinces and latitude. Rates were estimated using an inflection point of 65 My. (**A**) The difference between post- and pre-K/Pg origination rates ($\lambda_1 - \lambda_2$) declines significantly with increasing latitude. (**B**) Post-K/Pg origination rates (λ_1) decrease significantly with latitude. (**C**) Pre-K/Pg origination rates (λ_2) show no significant trend with latitude.
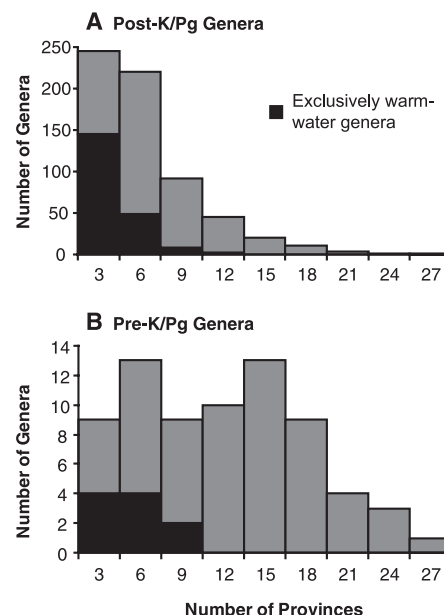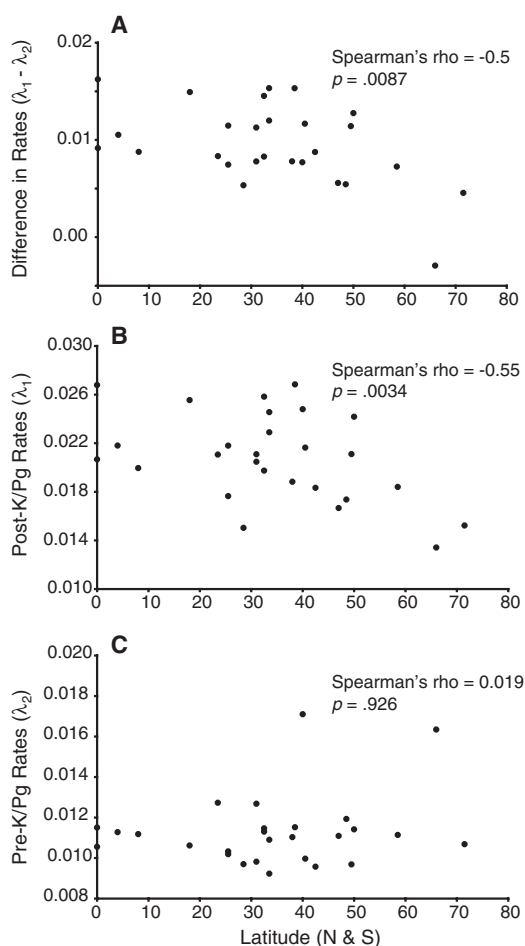
Fig. 4. Present-day geographic ranges of bivalve genera that originated (**A**) after or (**B**) before the K/Pg extinction. Genera originating before the K/Pg extinction (B) have significantly greater geographic ranges today, determined as the number of bioprovinces in which a genus occurs (median range of pre-K/Pg genera = 10 provinces, median range of post-K/Pg genera = 4 provinces, Kolmogorov-Smirnov test, $P = 2.16 \times 10^{-5}$), and significantly fewer exclusively warm-water genera than (A) genera originating after the K/Pg. Genera that exist exclusively in provinces with tropical or warm-temperate climates are denoted in black. All other genera have ranges extending into (but not necessarily restricted to) cold-temperate or polar provinces. The vast majority of such genera (91%) also occur in warm-water provinces.

and ongoing, so that the long-term shift in origination rate, and the spatial pattern of those originations, continues to structure the biological provinces of the modern world. Despite 65 My of evolutionary and environmental change, the modern marine biota, globally and regionally, bears the evolutionary and biogeographic imprint of the K/Pg event.

References and Notes

1. J. J. Sepkoski Jr., in *Global Events and Event Stratigraphy*, O. H. Walliser, Ed. (Springer, Berlin, 1996), pp. 35–52.
2. M. Foote, *J. Geol.* **111**, 125 (2003).
3. G. G. Mittelbach et al., *Ecol. Lett.* **10**, 315 (2007).
4. R. E. Ricklefs, *Ecol. Lett.* **7**, 1 (2004).
5. M. Foote, in *Evolutionary Patterns*, J. B. C. Jackson, S. Lidgard, M. L. McKinney, Eds. (Univ. of Chicago Press, Chicago, 2001), pp. 245–294.
6. C. M. Pease, *Paleobiology* **13**, 484 (1987).
7. See supporting material on *Science* Online.
8. D. Jablonski, K. Roy, J. W. Valentine, *Science* **314**, 102 (2006).
9. J. W. Valentine, D. Jablonski, A. Z. Krug, K. Roy, *Paleobiology* **34**, 169 (2008).
10. D. Jablonski, K. Roy, J. W. Valentine, R. M. Price, P. S. Anderson, *Science* **300**, 1133 (2003).
11. S. M. Kidwell, *Science* **307**, 914 (2005).
12. J. W. Valentine, D. Jablonski, S. Kidwell, K. Roy, *Proc. Natl. Acad. Sci. U.S.A.* **103**, 6599 (2006).
13. J. A. Crame, *Paleobiology* **28**, 184 (2002).
14. A. K. Behrensmeyer et al., *Paleobiology* **31**, 607 (2005).
15. J. A. Crame, *Paleobiology* **26**, 188 (2000).
16. M. L. Reaka, P. J. Rodgers, A. U. Kudla, *Proc. Natl. Acad. Sci. U.S.A.* **105**, 11474 (2008).
17. S. T. Williams, T. F. Duda, *Evolution* **62**, 1618 (2008).
18. D. M. Raup, *Paleobiology* **4**, 1 (1978).
19. D. M. Raup, *Paleobiology* **1**, 333 (1975).
20. J. J. Sepkoski Jr., *Bull. Am. Paleontol.* **363**, 1 (2002).
21. A. I. Miller, J. J. Sepkoski Jr., *Paleobiology* **14**, 364 (1988).
22. D. M. Raup, D. Jablonski, *Science* **260**, 971 (1993).
23. K. Roy, E. E. Goldberg, *Am. Nat.* **170**, S71 (2007).
24. R. E. Ricklefs, *Trends Ecol. Evol.* **22**, 601 (2007).
25. R. E. Ricklefs, J. B. Losos, T. M. Townsend, *J. Evol. Biol.* **20**, 1751 (2007).
26. S. Nee, *Annu. Rev. Ecol. Evol. Syst.* **37**, 1 (2006).
27. S. Nee, *Evolution* **55**, 661 (2001).
28. S. Nee, *Paleobiology* **30**, 172 (2004).
29. M. Foote, *Paleobiology* **26** (suppl.), 74 (2000).
30. J. Alroy et al., *Science* **321**, 97 (2008).
31. S. M. Stanley, *Paleobiology* **34**, 1 (2008).
32. G. J. Vermeij, *Evolution and Escalation* (Princeton Univ. Press, Princeton, NJ, 1987).
33. We thank M. Foote, S. M. Kidwell, T. D. Price, K. Roy, and three anonymous reviewers for comments and M. Foote for programming assistance. This research was supported by NASA.

A Great-Appendage Arthropod with a Radial Mouth from the Lower Devonian Hunsrück Slate, Germany

Gabriele Kühl,[1] Derek E. G. Briggs,[2] Jes Rust[1]

Great-appendage arthropods, characterized by a highly modified anterior limb, were previously unknown after the Middle Cambrian. One fossil from the Lower Devonian Hunsrück Slate, Germany, extends the stratigraphic range of these arthropods by ~100 million years. *Schinderhannes bartelsi* shows an unusual combination of anomalocaridid and euarthropod characters, including a highly specialized swimming appendage. A cladistic analysis indicates that the new taxon is basal to crown-group euarthropods and that the great-appendage arthropods are paraphyletic. This new fossil shows that features of the anomalocaridids, including the multisegmented raptorial appendage and circular plated mouth, persisted long after the initial radiation of the euarthropods.

A range of Cambrian arthropods share a prominent limb at the front of the head referred to as the "great appendage" (*1*). They include the Anomalocarididae and Cambrian euarthropods such as *Yohoia*, *Leanchoilia*, *Jiangfengia*, and *Fortiforceps* and are usually interpreted as a paraphyletic group within the crown, basal to chelicerates, and the great appendage to be homologous with the chelicera of living chelicerates (*1–6*). Alternatively, they have been considered basal to the crown-group euarthropods, in which case the great appendage has been lost in living taxa (*7, 8*). Here, we describe a great-appendage arthropod from the famous Lower Devonian Hunsrück Slate (*9*). This arthropod shows a previously unseen combination of the characters that occur in Cambrian anomalocaridids and euarthropods.

Schinderhannes bartelsi, a new genus and species, is a representative of the stem lineage of the Euarthropoda. The name *Schinderhannes* is derived

[1]Division of Palaeontology, Steinmann Institute, University of Bonn, Nussallee 8, 53115 Bonn, Germany. [2]Department of Geology and Geophysics, and Yale Peabody Museum of Natural History, Yale University, Post Office Box 208109, New Haven, CT 06520–8109, USA.

from an 18th-century bandit in the Hunsrück area and *bartelsi* is a tribute to Christoph Bartels of Bochum, Germany, an authority on the Hunsrück Slate fossils. The material is a single specimen: PWL 1994/52-LS is the holotype, located at the Naturhistorisches Museum Mainz. The specimen has been x-radiographed (Fig. 1F), drawn (Fig. 1, B and D), and reconstructed (Fig. 1G). It was discovered in the Hunsrück Slate, Germany, at the Eschenbach-Bocksberg Quarry in Bundenbach (*10*); it was found in the Lower Devonian Kaub Formation.

Diagnosis. The head bears a preoral great appendage with at least nine podomeres, a radial mouth, and huge eyes. Podomeres three to nine of the great appendage bear an elongate lateral spine, and podomeres four to nine have a long, ventral, comb-like projection. An additional large triangular flaplike appendage at the rear of the head is thickened along its margin. The trunk consists of 12 segments: The first 10 have tergites and bear biramous appendages, the 11th bears a lateral flukelike appendage, and the 12th is apodous. The trunk terminates in a long tail spine.

Description. The total length, including the tail spine, is 98 mm. The specimen (Fig. 1, A and B) is oriented parallel-oblique to the bedding so that the ventral side shows the left eye in outline and reveals the outer surface of the left edge of the trunk tergites (fig. S1, C and D). Some features, such as the head shield, are obscured by incomplete pyritization and phosphatization. The outline of the large postoral head appendage has been affected by flattening: The left is foreshortened as compared with the right, which shows striking evidence of wrinkling. This appendage is difficult to interpret without additional examples preserved in other attitudes to the bedding.

The body is divided into head and trunk. The head bears a pair of preoral great appendages (Fig. 1, B to E, and fig. S1A), a circular mouth structure, a pair of huge eyes, and a pair of flaplike limbs at the rear. Although there is no clear evidence of a head shield, the presence of dorsal tergites in the trunk region suggests that one was present (fig. S1D).

The great appendage (A1) (Fig. 1, B and E, and fig. S1A) consists of up to nine podomeres. Podomeres one and two are short and wide, whereas podomere three is three times longer and bears a lateral spine (Fig. 1, E and G). Podomeres four to nine also bear a long inwardly projecting lateral spine and a long parallel-sided ventral projection that extends at a high angle to the appendage (Fig. 1, B, E, and G, and fig. S1A). This projection decreases in length from the fourth to the ninth podomere. Each one bears a series of up to five or six regularly spaced orthogonal spines along its length, decreasing in number on the more distal podomeres. A subcircular mouth ring (Fig. 1, F and H, and fig. S1B) is concealed by the ventral projections. A series of small subtriangular features, particularly on the left side, may represent tooth plates. Differences in width may reflect its attitude to the bedding.

The stalked eyes are positioned laterally behind the great appendages. The left eye indicates a suboval outline, although it is affected by flattening. The eyes are covered in numerous tiny, close-packed, hexagonal lenses (fig. S1C).